



HAL
open science

Anomalous Complex Electrical Conductivity of a Graphitic Black Schist From the Himalayas of Central Nepal

Jana H. Börner, Frédéric Girault, Mukunda Bhattarai, Lok Bijaya Adhikari, Damien Deldicque, Frédéric Perrier, Klaus Spitzer

► **To cite this version:**

Jana H. Börner, Frédéric Girault, Mukunda Bhattarai, Lok Bijaya Adhikari, Damien Deldicque, et al.. Anomalous Complex Electrical Conductivity of a Graphitic Black Schist From the Himalayas of Central Nepal. *Geophysical Research Letters*, 2018, 45, pp.3984-3993. 10.1029/2018GL077178 . insu-03589356

HAL Id: insu-03589356

<https://insu.hal.science/insu-03589356>

Submitted on 25 Feb 2022

HAL is a multi-disciplinary open access archive for the deposit and dissemination of scientific research documents, whether they are published or not. The documents may come from teaching and research institutions in France or abroad, or from public or private research centers.

L'archive ouverte pluridisciplinaire **HAL**, est destinée au dépôt et à la diffusion de documents scientifiques de niveau recherche, publiés ou non, émanant des établissements d'enseignement et de recherche français ou étrangers, des laboratoires publics ou privés.

Copyright

RESEARCH LETTER

10.1029/2018GL077178

Key Points:

- Complex conductivity of black schist and augen gneiss from Nepal was investigated in the laboratory
- Black schist shows high polarizability and anisotropy due to disseminated, aligned graphite plates
- Neglecting complex conductivity during inversion can lead to misinterpretation of MT surveys

Supporting Information:

- Supporting Information S1

Correspondence to:

J. H. Börner,
jana.boerner@geophysik.tu-freiberg.de

Citation:

Börner, J. H., Girault, F., Bhattarai, M., Adhikari, L. B., Deldicque, D., Perrier, F., & Spitzer, K. (2018). Anomalous complex electrical conductivity of a graphitic black schist from the Himalayas of central Nepal. *Geophysical Research Letters*, 45, 3984–3993.
<https://doi.org/10.1029/2018GL077178>

Received 23 JAN 2018

Accepted 5 APR 2018

Accepted article online 19 APR 2018

Published online 11 MAY 2018

Anomalous Complex Electrical Conductivity of a Graphitic Black Schist From the Himalayas of Central Nepal

Jana H. Börner¹ , Frédéric Girault² , Mukunda Bhattarai³, Lok Bijaya Adhikari³, Damien Deldicque⁴, Frédéric Perrier², and Klaus Spitzer¹

¹Institute of Geophysics and Geoinformatics, TU Bergakademie Freiberg, Freiberg, Germany, ²Institut de Physique du Globe de Paris, Sorbonne Paris Cité, University Paris Diderot, CNRS, Paris, France, ³National Seismological Centre, Department of Mines and Geology, Lainchaur, Kathmandu, Nepal, ⁴Laboratoire de Géologie de l'ENS - PSL Research University - UMR 8538 CNRS, Paris, France

Abstract We analyzed in the laboratory the frequency-dependent, complex-valued, electrical conductivity of a graphitic black schist and an augen gneiss, both collected in the Main Central Thrust shear zone in the Himalayas of central Nepal, which was heavily affected by the deadly Mw7.8 Gorkha earthquake in 2015. We focused on anisotropy and salinity dependence of both cores and crushed material as well as the impact of CO₂ on conductivity. This black schist possesses an extraordinarily high polarizability and a highly frequency-dependent conductivity. Its anisotropy is very pronounced. The investigations can relate the main polarization feature to disseminated, aligned plates of graphite. By contrast, the augen gneiss shows low polarizability and a moderately anisotropic conductivity dominated by the pore-filling brine. We further demonstrate that neglecting the complex and frequency-dependent nature of conductivity can lead to serious misinterpretation of magnetotelluric data during inversion if highly polarizable rocks are present.

Plain Language Summary We investigated the electrical properties of a graphitic black schist and an augen gneiss, both collected in a shear zone in the Himalayas of central Nepal, which was heavily affected by the deadly Ghorka earthquake in 2015 (moment magnitude Mw7.8). We focused on electrical resistivity, polarization, anisotropy, and the influence of pore water salinity. Both cores and crushed material were analyzed, which allows for a more detailed understanding of the mechanisms of electric conduction in such rocks. The black schist shows a strongly frequency-dependent resistivity, which is associated with an extraordinarily high polarization. Its anisotropy is very pronounced. Scanning electron microscope images confirm that this behavior is due to disseminated, aligned plates of graphite. The augen gneiss on the other hand shows a regular electrical resistivity, which is dominated by the pore-filling brine. Besides the new insights in the mechanisms of electric conduction in these unusual, highly metamorphic rocks, our investigations bear relevance for large-scale geophysical surveys aiming at revealing the internal structure of the Himalayas and understanding the occurrence of large earthquakes in the area. We demonstrate that neglecting the unusual electrical properties of the black schist during interpretation of influenced data can lead to serious misinterpretation.

1. Introduction

The Himalayan Range, frequently affected by large earthquakes, results from the collision of the Indian plate with Eurasia. The tectonic process essentially takes place along a single subhorizontal fault, the Main Himalayan Thrust (MHT). The MHT exhibits a ramp, which blocks all motion, except during large earthquakes. The Main Central Thrust (MCT) shear zone, which branches at depth on the MHT, places high-grade metamorphic rocks of the Greater Himalayan Sequence, located northward, over low-grade metamorphic rocks of the Lesser Himalayan Sequence (e.g., Bollinger et al., 2004; Sapkota et al., 2013; Upreti, 1999).

In the last two decades, multiple magnetotelluric (MT) surveys have been conducted perpendicular to the MHT and MCT, most of which image midcrustal conductive zones, partially associated with seismic activity (e.g., Arora et al., 1982; Israil et al., 2008; Lemonnier et al., 1999; Pavan Kumar et al., 2014; Rawat et al., 2014;

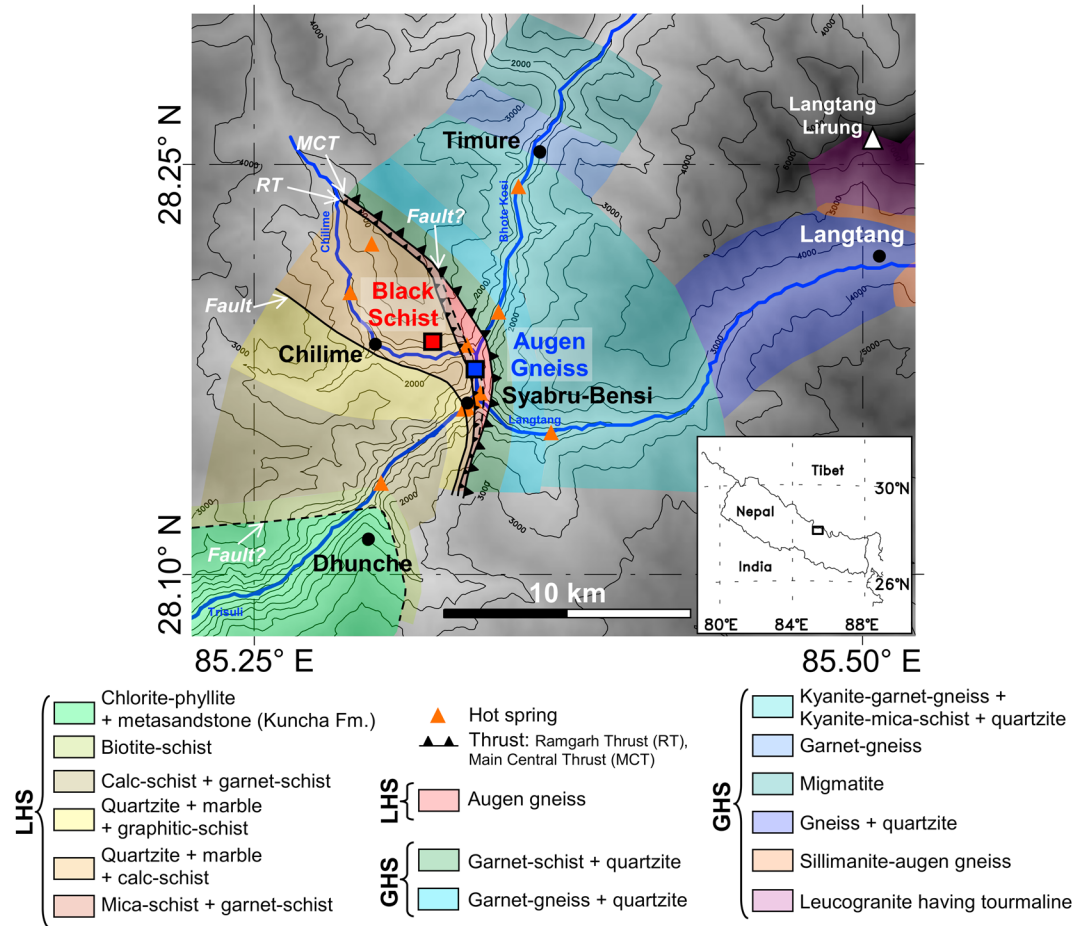


Figure 1. Geological map of the upper Trisuli and Langtang valleys (central Nepal) showing the sampling locations in the Lesser Himalayan Sequence (LHS): Augen gneiss (blue) and black schist (red). Orange triangles indicate the location of hot springs. The inset shows the sampling area in Nepal. Geology is mapped from various contributions (see Girault et al., 2012 and references therein). Topographic contours are smoothed from the Shuttle Radar Topography Mission Digital Elevation Model (courtesy of Laurent Bollinger). GHS = Greater Himalayan Sequence.

Unsworth, 2010; Unsworth et al., 2005). Apart from recent investigations, which aim at the reproducibility and numerical stability of said anomalies (Sailhac et al., 2016), different explanatory approaches are available to explain the presence of a deep conductive zone. The zone might be associated either with the presence of highly conductive brines or with the increased occurrence of conductive phases such as graphitic mineralization (e.g., Beyssac et al., 2004; Groppo et al., 2013), which are known to sometimes bear anomalous electrical properties (e.g., Duba et al., 1988; Jödicke, 1992; Jödicke et al., 2004). In recent years, large carbon dioxide (CO₂) discharges with a metamorphic isotopic signature were discovered and studied in detail on the surface (Girault et al., 2014). The combined observations suggest that carbon, indeed, could play an important role in the crustal conductivity structure of the area.

To evaluate this possibility, we analyzed in the laboratory the electrical conductivity of two Himalayan metamorphic rock samples—a black schist and an augen gneiss—collected in the CO₂ degassing area associated with the MCT approximately 60 km north of Kathmandu, in the region affected by the deadly Mw7.8 2015 earthquake (Figure 1). We carried out laboratory measurements of the complex-valued electrical conductivity of the Himalayan rocks, thereby focusing on anisotropy and salinity dependence. Understanding the electrical properties of the Himalayan rocks may provide valuable information, which might help to enhance both the interpretation of deep crustal geophysical surveys and our understanding of the Himalayan orogeny.

2. Electrical Rock Properties and CO₂

The electrical rock conductivity σ^* — the reciprocal of electrical rock resistivity ρ^* — in general is a complex and frequency-dependent quantity and originates from both electrolytic (σ_{el}) and interface (σ_{if}^*) conduction mechanisms (e.g., Olhoeft, 1979):

$$\sigma^*(\omega) = \frac{1}{\rho^*(\omega)} = \sigma_{el} + \sigma_{if}^*(\omega), \quad (1)$$

where ω is the angular frequency, and $*$ denotes complex quantities. The combination of the real-valued σ_{el} and the complex-valued σ_{if}^* causes the measurable overall rock conductivity to be complex and frequency dependent. Complex rock conductivity may be written as real and imaginary part (σ' and σ'' , respectively) or as magnitude ($|\sigma^*|$) and phase shift (φ):

$$\sigma^*(\omega) = \sigma'(\omega) + i\sigma''(\omega) = (\sigma_{el} + \sigma'_{if}(\omega)) + i\sigma''_{if}(\omega) \quad (2)$$

$$= |\sigma^*| \cdot e^{i\varphi} \quad (3)$$

with i being the imaginary unit and

$$\varphi = \arctan\left(\frac{\sigma''}{\sigma'}\right). \quad (4)$$

The real-valued (frequency independent) electrolytic conductivity σ_{el} depends on pore space characteristics, saturation, and pore water salinity and is usually described by Archie's law (Archie, 1942; Schön, 2015).

In silicate rocks, the complex and frequency-dependent interface conductivity σ_{if}^* is caused by the electrical double layer, which forms at the contact of mineral grains and the conductive pore water. As a consequence of its origin, σ_{if}^* depends on the inner surface area, pH, and also on salinity (e.g., F. D. Börner & Schön, 1991; Revil & Skold, 2011; Skold et al., 2011; Weller & Slater, 2012). It depends less strongly on water saturation and salinity than the electrolytic conductivity (e.g., Breede et al., 2012; Vinegar & Waxman, 1984).

An additional polarization mechanism — the so called electrode polarization — may be observed when electronically conductive minerals, such as, for example, pyrite, chalcopyrite, and graphite are present in a significant amount. The transfer from electrolytic (ion transport) to electronic (electron transport) conduction causes a strong charge separation at the surface of the mineral grains (e.g., Pelton et al., 1978; Revil et al., 2015). Often, the polarization for one characteristic polarizable feature appears as a pronounced peak in both σ'' and φ and may be described by the Cole-Cole model (Cole & Cole, 1941; Pelton et al., 1978):

$$\frac{1}{\sigma^*(\omega)} = \frac{1}{\sigma_0} \left[1 - m \left(1 - \frac{1}{1 + (i\omega\tau)^c} \right) \right], \quad (5)$$

where σ_0 denotes the conductivity asymptote toward zero frequency, m is chargeability and reflects the polarization strength in terms of phase shift, τ is the relaxation time and indicates the period of maximum polarization, and c is the frequency exponent and describes the broadness of the polarization peak. Motivated by his studies on numerous mineral deposits containing both graphite and/or pyrite, Pelton et al. (1978) extended this model for two coexisting polarizable components (indices 1 and 2, respectively):

$$\frac{1}{\sigma^*(\omega)} = \frac{1}{\sigma_0} \left[1 - m_1 \left(1 - \frac{1}{1 + (i\omega\tau_1)^{c_1}} \right) \right] \left[1 - m_2 \left(1 - \frac{1}{1 + (i\omega\tau_2)^{c_2}} \right) \right]. \quad (6)$$

Pelton et al. (1978) found graphite deposits to be characterized by high chargeabilities (above 0.7) and long relaxation times ($10^2 - 10^4$ s). Pyrite deposits showed a wide range of relaxation times and chargeabilities (generally below 0.8) depending on pyrite grain size and volumetric content. Basically, equation (6) may be generalized to an arbitrary number of polarizable components.

The presence of CO₂ acts on σ^* because the presence of the reactive gas in pore space gives rise to a network of physicochemical processes (J. H. Börner et al., 2013). First, a free CO₂ phase causes partial water saturation. Furthermore, CO₂ is highly soluble in water, partly dissociates and consequently acts on pore water conductivity σ_w . Laboratory experiments showed that these processes cause complex changes of σ_w (J. H. Börner et al., 2015). Also, the pH decreases, when no buffering occurs. All processes act at once on σ^* during interaction of water-bearing rocks and CO₂ (J. H. Börner et al., 2017).

Table 1
Overview of Sample Characteristics

Sample	#	Porosity	Spec. internal surface	Fluid conductivity	Mineral composition
Black schist					
Core	2	4.6% ± 1.1%	1.7 ± 1.5 m ² /g	0.108 ± 0.003 S/m	61.9 ± 12.4% quartz 16.2 ± 3.2% phlogopite
Core ⊥	3	8.6% ± 1.1%			11.6 ± 2.3% muscovite 6.3 ± 1.3% graphite 3.9 ± 0.8% pyrite
Crushed	6	43.7% ± 2.1%	21.2 ± 0.7 m ² /g	0.0036 ... 12.01 S/m	
Black schist-quartz sand mixtures					
Crushed	7	33.7% ± 4.82%	0.61 ... 21.2 m ² /g	0.101 ± 0.004 S/m	
Augen gneiss					
Core	2	1.9% ± 0.50%	0.6 ± 0.4 m ² /g	0.118 ± 0.009 S/m	37.2 ± 5.7% quartz 35.9 ± 5.5% albite
Core ⊥	2	2.6% ± 0.88%			26.9 ± 4.1% phlogopite traces of microcline, apatite, uraninite
Crushed	5	38.1% ± 2.5%	2.1 ± 0.1 m ² /g	0.014 ... 12.17 S/m	

Note. Fluid conductivity is given at 20°C, composition in wt%. Core porosities and internal surfaces vary within one rock type due to sample individuality.

3. Materials and Methods

The focus of the laboratory study was on the electrical properties of a biotite-rich, black mica schist (Proterozoic to Middle Proterozoic age), which contains 6.3 ± 1.3% of graphite and 3.9 ± 0.8% of pyrite as (electronically) conductive and polarizable components (obtained from X-ray diffraction analysis, Scanning electron microscopy, and Raman spectroscopy). For comparison, we also investigated a quartz-feldspar-biotite-muscovite-tourmaline augen gneiss (Paleoproterozoic to Early Proterozoic age; Kohn et al., 2010), which is common in the area of interest and does not contain strongly polarizable minerals. The specific inner surface area was determined using the nitrogen adsorption method. An overview of the investigated samples and their characteristics is given in Table 1.

Both massive pieces and crushed material were investigated (Figures 2a and 2b). From the massive rocks, core plugs of 2-cm diameter and 3-cm length were drilled both parallel and perpendicular to the natural foliation. The supplementation of our investigations by crushed samples allows for a better understanding of the conduction mechanisms.

Both black schist and augen gneiss possess a relatively low fissure porosity, which is nevertheless sufficiently high to allow for enough contact between water phase and mineral components to access the polarization properties of the material. The crushed samples naturally show a very high porosity. The specific inner surface area is similar and moderately high for both solid rocks. However, the crushed samples show significant differences with regard to their inner surface area. The inner surface area of the crushed schist is larger than that of the crushed gneiss by one order of magnitude.

The complex conductivity was measured in the frequency range between 10⁻³ and 10⁴ Hz with a SIP Fuchs III measuring device from Radic Research (Germany) for all samples saturated with $\sigma_w = 0.1$ S/m at 20°C NaCl solution (see supporting information S1). In addition, multivalinity experiments were carried out in order to determinate the order of magnitude of the real part of interface conductivity σ'_{if} (cf. equations (1) and (2), Revil & Skold, 2011; Waxman & Smits, 1968). In addition, measurements on black schist-quartz sand mixtures were carried out in order to investigate the minimum mass fraction of black schist necessary to dominate the bulk

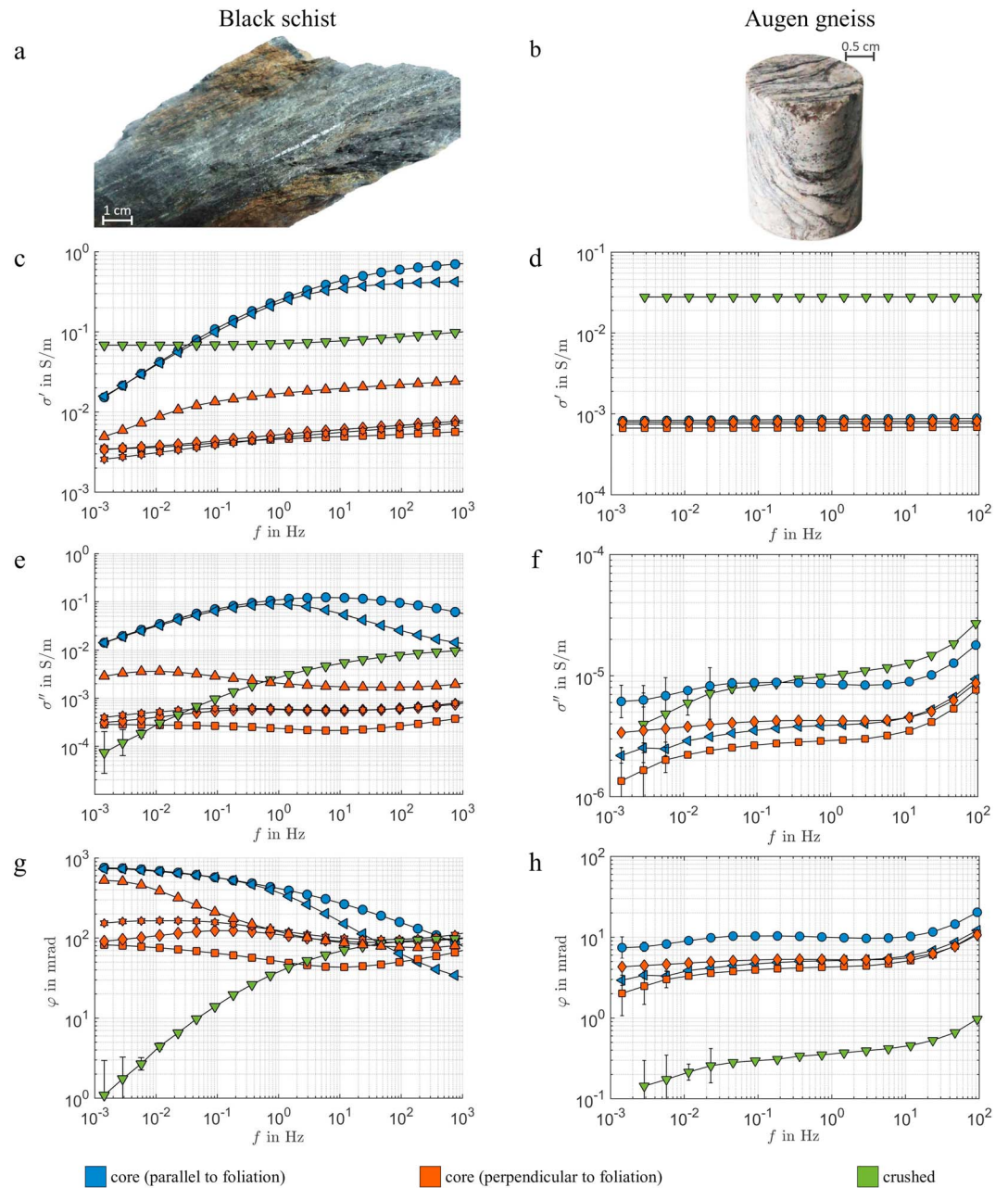


Figure 2. Frequency-dependent complex conductivity of the black schist (a, left column) and the augen gneiss (b, right column) in terms of real part conductivity (c and d), imaginary conductivity (e and f) and phase shift (g and h). Varying markers indicate the sample specimen; lines are just for visual guidance. All samples were saturated with a NaCl solution ($\sigma_w = 0.1$ S/m). For further experimental details see Table 1.

properties. By way of example, experiments, where the crushed material was exposed to a CO_2 atmosphere at 5-MPa hydrostatic pressure and 30°C for 7 days, were conducted to qualitatively assess the impact of CO_2 on the SIP response of the investigated rocks (see supporting information S5). These experiments were carried out with the apparatus described in detail by J. H. Börner et al. (2017).

4. Results

4.1. Anisotropic Conductivity of Core Samples

The complex, frequency-dependent conductivity data of all cores and the crushed samples at $\sigma_w = 0.1$ S/m are shown in Figure 2 in terms of σ' , σ'' , and φ (top to bottom). The black schist (left column) shows

highly anomalous electrical properties. The most prominent feature for all black schist cores drilled parallel to the foliation (blue in Figure 2, left column) is the low-frequency polarization, which shows up as a peak in both the imaginary conductivity (approximately 0.1 S/m around 1 Hz) and the phase shift (approximately 750 mrad around 10^{-3} Hz) as well as the frequency dependence of real conductivity, which covers up to two orders of magnitude. The strong polarizability also results in generally high conductivity values in the covered frequency range compared to the relatively low porosity of 1.9–8.6%. This combination of σ' , σ'' , and φ can be explained by a polarization of the Cole-Cole type (cf. equation (5)). This polarization feature is characterized by a relaxation time τ of $3 \cdot 10^4$ s, a chargeability m of 0.997 and a frequency exponent c of 0.51. The Cole-Cole fitting is demonstrated in supporting information S2. Given the physical bounds of m , which is between 0 and 1, the chargeability is extremely high. Also, the frequency exponent is close to 0.5, which is the typical value for electrode polarization phenomena (so-called Warburg impedance; Warburg, 1899). Together with the long relaxation time and in relation to the results of Pelton et al. (1978), the low-frequency polarization can be interpreted as originating from the 6.9% of graphite in the black schist.

Further information on the textural appearance of the graphite may be gained from assessing the electrical anisotropy. Compared with the parallel cores, cores drilled perpendicular to the foliation (orange in Figure 2, left column) show a reduced polarization (σ' variation in frequency of a factor up to 5 and φ from 80 to 525 mrad). The low-frequency graphite-associated polarization identified from the parallel cores is also present for the perpendicular cores (see supporting information S2).

At the same time, a second contribution at higher frequencies is observed. Analyzing the perpendicular core data by means of the double Cole-Cole model (cf. equation (6)) indicates a polarization feature with τ between $3 \cdot 10^{-3}$ to $3 \cdot 10^{-4}$ s, m ranging from 0.2 to 0.3 and an exponent c of about 0.4 (see table in the supporting information S2). Going back to the parallel cores, this second contribution may also be found, but due to the pronounced graphite-associated polarization it is partially masked. The origin of this second polarization feature cannot clearly be identified. It could be associated to the 3.9% of pyrite (the observed τ and m fit to the data set of Pelton et al. (1978), for pyrite deposits) or to the polarization of all silicate mineral surfaces.

The highly anisotropic measurements of the black schist cores indicate that the graphite particles are arranged according to the foliation without forming connected bands. If connected bands were present, this would show up as a dominating ohmic (i.e., real valued and frequency independent) conductivity contribution. Since the polarization effects dominate the black schist properties, the graphite seems to be disseminated and only loosely aligned along with the foliation. These interpretations are confirmed by scanning electron microscope images (see supporting information S4).

For comparison, the abundant augen gneiss (right column in Figure 2) shows weak polarization, which manifests itself in a small imaginary conductivity ($1 \cdot 10^{-6}$ – $1 \cdot 10^{-5}$ S/m) and phase shift (3–10 mrad). No polarization peak appears, and consequently, the frequency dependence of all conductivity components is low. These characteristics indicate that the complex conductivity of the augen gneiss is dominated by electrolytic processes. This observation is in good agreement with the absence of polarizable mineral components (cf. Table 1).

Despite the macroscopically visible foliation, the electrical anisotropy of the augen gneiss is weak. A tendency to higher conductivity and polarization along the foliation may be seen, but it is in the same range as the individual variety of the core specimen for the presented data set.

4.2. Conductivity of Crushed Material

Crushing of the solid rock material results in samples possessing the same mineral content like the original rock, but none of its structural and textural properties. Therefore, comparing σ^* of both solid and crushed material allows to identify texture-driven polarization features.

Such an effect may be observed for the black schist (cf. green curves in left column of Figure 2). The low-frequency polarization described above is lost due to crushing (σ'' drops by 2.5 orders of magnitude at 10^{-3} Hz, φ drops by almost 3 orders of magnitude). This implies that a large part of the electrical conduction is associated with the texture of the solid core material, which further backs up the interpretation of the aligned graphite plates being the polarization source.

In case of the augen gneiss, the crushing procedure has no effect on the general characteristics of the σ^* frequency dependence. This observation leads to the conclusion that the polarization effects present in the augen gneiss are driven by volume effects and do not significantly depend on the texture of the solid material.

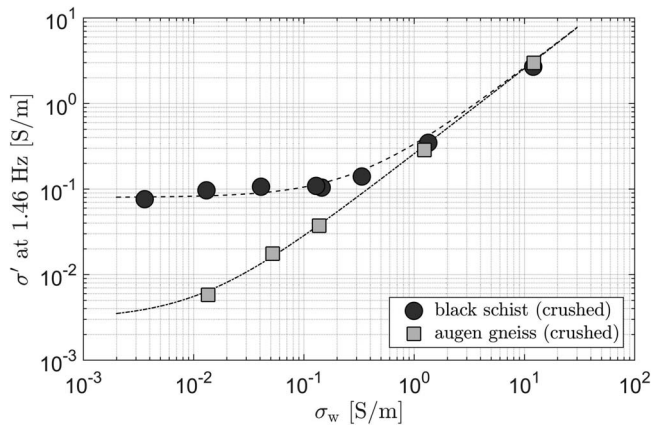


Figure 3. Salinity dependence of real part conductivity derived from multisalinity experiments on crushed samples. The low salinity asymptote of the real part of interface conductivity σ'_{if} is $8 \cdot 10^{-2}$ S/m for the black schist and $3 \cdot 10^{-3}$ S/m for the augen gneiss.

A moderate increase of σ'' compared to the core samples is related to the increased accessibility of inner surface area (cf. Table 1).

To further investigate the relationship between water conductivity (i.e., salinity) and rock conductivity, we carried out multisalinity measurements on crushed samples of both black schist and augen gneiss. The results are shown in Figure 3 in terms of the real conductivity σ' at 1.46 Hz. The slope of the curves represents the reciprocal of the formation factor F (cf. Archie, 1942), whereas the intercept with the y axis is the real part of surface conductivity σ'_{if} (cf. Revil & Skold, 2011; Waxman & Smits, 1968).

The investigations show that both black schist and augen gneiss have a comparable formation factor, which is due to the similar porosity and particle size of the crushed samples. The real part of surface conductivity, however, differs by a factor of almost 30 between the rocks. The augen gneiss exhibits a low surface conductivity—as found in the complex conductivity as well—and is mainly dominated by the Archie behavior. On the other hand, the black schist shows an extremely high real surface conductivity, which dominates rock conductivity over a wide range of salinities.

Furthermore, measurements on black schist-quartz sand mixtures demonstrated that already rather low mass fractions (approximately 25%) of black schist can dominate the bulk properties of the whole material (see supporting information S3).

5. Discussion and Conclusions

The investigated rocks bear anomalous and highly indicative electrical properties. The black schist is characterized by strong anisotropy and frequency dependence of conductivity. The complex conductivity measurements and accompanying analyses suggest that graphite is the main source of polarization and is disseminated within the black schist but with a preferred orientation along the natural foliation. By contrast, the augen gneiss is characterized by a strong domination of electrolytic conduction and low surface conduction. Consequently, gneiss formations are more sensitive to changes in brine salinity than black schist formations.

Quantitative deductions of field-scale effects from laboratory data are difficult and error prone due to:

1. the heterogeneity of rocks, which cannot be covered by a limited set of samples,
2. the variability of local bedding, which tends to average out small-scale anisotropy and strong contrasts,
3. influencing factors, which cannot be covered by the small samples, such as macroscopic fractures,
4. the influence of sampling procedure (depressurization, drilling, ...) on the rock properties.

Nevertheless, general tendencies and qualitative indications may be formulated on the basis of the laboratory data set. The conductivity of the black schist, which is characterized by strong polarization and anisotropy, is likely to show such features to some extent also in geophysical imaging. The weak salinity dependence of the black schist conductivity due to the dominance of surface conduction is probably also present on a larger scale. Consequently, a formation with high conductivity might be misinterpreted in terms of brine conductivity when the surface conduction and polarization effects are not taken into account.

On the other hand, the low polarization and dominant electrolytic conduction in the augen gneiss implies that inferring brine conductivity from electrical measurements (for known porosity and temperature) should be well possible for gneiss formations. The characterization of the investigated augen gneiss by means of a real-valued and frequency-independent conductivity is probably sufficient for large-scale studies.

Particular caution is required when electromagnetic field data acquisition takes place in the sphere of influence of a highly polarizable rock such as the black schist. The frequency-dependent conductivity implies that a black schist formation may appear differently at different frequencies (and therefore depths after inversion) of electromagnetic surveys such as MT or controlled source electromagnetics, but also airborne electromagnetics and transient electromagnetics (e.g., Esposito et al., 2017; Manca & Viezzoli, 2018; Marchant et al., 2018; Stoyer, 1976). Neglecting this during inversion of affected field data can result in erroneous conductivity models, an effect demonstrated in Figure 4. For this synthetic test, a horizontal 25-m-thick layer of black schist

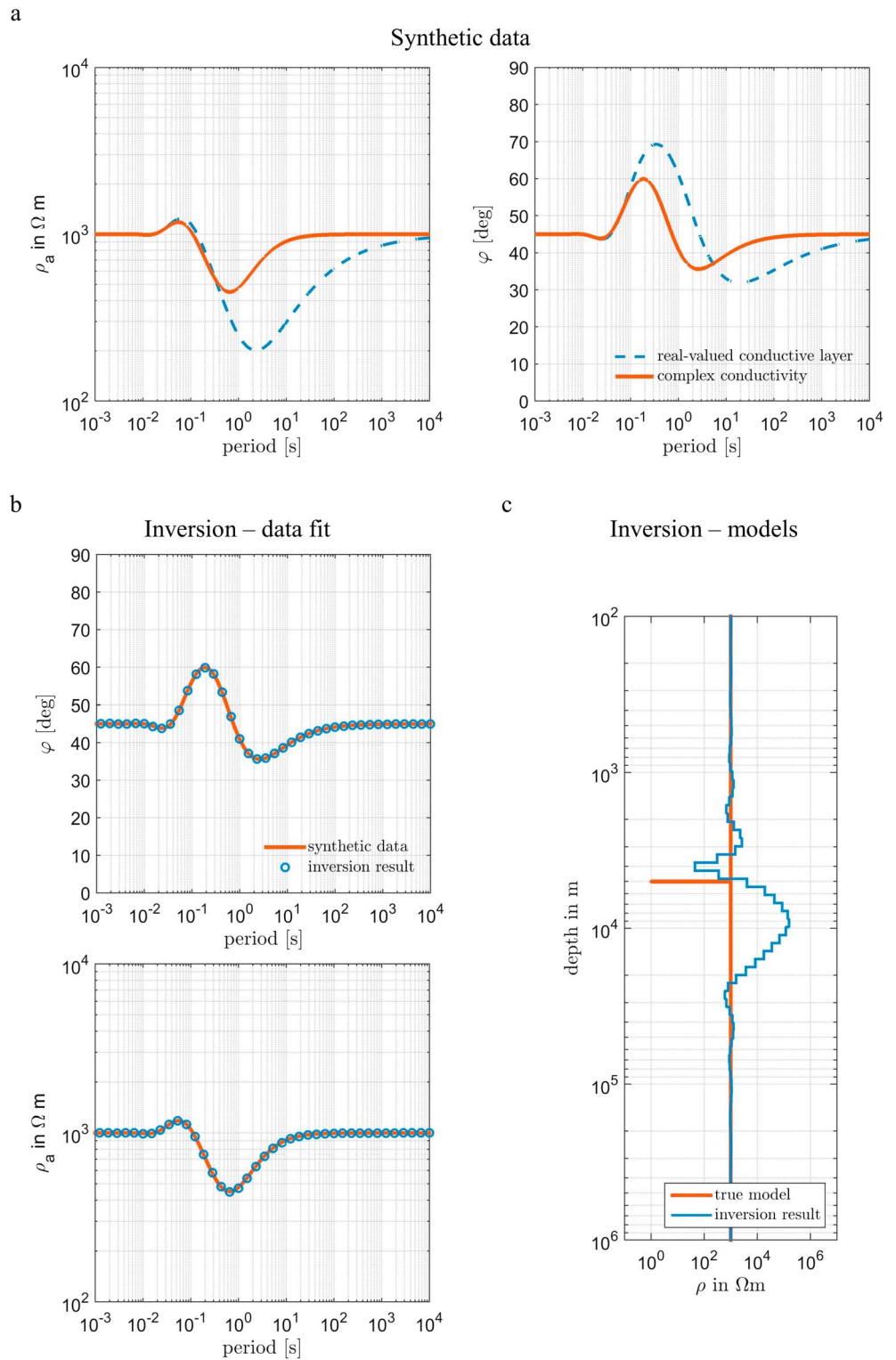


Figure 4. Demonstration of the effect of complex conductivity on magnetotelluric data and inversion. (a) Comparison between synthetic magnetotelluric data including a 25-m black schist layer ($\sigma_0 = 1.22 \cdot 10^{-3}$ S/m, $m = 0.997$, $\tau = 3 \cdot 10^4$ s, $c = 0.51$) at 5,000-m depth (orange line) and a real-valued, conductive layer (1 S/m) of same thickness (blue, dashed line). (b) Data fit for the inversion of synthetic data while neglecting complex conductivity. (c) Comparison between true model and inversion result.

(σ^* represented by the Cole-Cole model given in line 1 of supporting information Table S1) is embedded in a 10^{-3} S/m homogeneous Earth at 5,000-m depth. Synthetic MT data are calculated and then inverted by means of a forward operator, which works with scalar, real-valued conductivity only (for details, see supporting information S6). The inversion is capable of fitting the data remarkably well (maximum deviation for both ρ_a and $\varphi < 1\%$), and the resulting model is geologically possible. However, it completely fails to reconstruct the anomalous layer and contains artifacts in order to compensate for the frequency dependence of σ^* .

Overall, the presented laboratory results are important prior information to constrain our understanding of the electrical properties of the Himalayan metamorphic rocks. This information will help to reveal the nature of conductivity anomalies detected along the mountain range by large-scale geophysical surveys. Furthermore, understanding the physics of conductive phases in metamorphous rocks in the presence of CO₂ opens important new perspectives in studying CO₂ production and migration in mountain building areas.

Acknowledgments

Jana H. Börner thanks for funding by the German Research Foundation (DFG, grant SP 356/14-1). The authors thank Volker Herdegen for the accompanying analyses and the assistance during the high-pressure experiments. The authors also thank Rajendra Khanal, Director General of Department of Mines and Geology, Nepal, and Soma Nath Sapkota, Deputy Director General for support and authorizations. Furthermore, our thanks go to Langtang National Park authorities for entry and sampling permission. We sincerely thank Volker Rath and one anonymous reviewer for their comments and questions, which helped to improve this manuscript. All presented experimental data are listed in the tables and supporting information. This is IPGP contribution number 3934.

References

- Archie, G. E. (1942). The electrical resistivity log as an aid in determining some reservoir characteristics. *Transactions of the American Institute of Mining, Metallurgical and Petroleum Engineers*, 146(146), 54–62.
- Arora, B. R., Lilley, F. E. M., Sloane, M. N., Singh, B. P., Srivastava, B. J., & Prasad, S. N. (1982). Geomagnetic induction and conductive structures in north-west India. *Geophysical Journal International*, 69(2), 459–475.
- Beysac, O., Bollinger, L., Avouac, J.-P., & Goffé, B. (2004). Thermal metamorphism in the lesser Himalaya of Nepal determined from Raman spectroscopy of carbonaceous material. *Earth and Planetary Science Letters*, 225, 233–241.
- Bollinger, L., Avouac, J. P., Cattin, R., & Pandey, M. R. (2004). Stress buildup in the Himalaya. *Journal of Geophysical Research*, 109, B11405. <https://doi.org/10.1029/2003JB002911>
- Börner, F. D., & Schön, J. H. (1991). A relation between the quadrature component of electrical conductivity and the specific surface area of sedimentary rocks. *Log Analyst*, 32, 612–613.
- Börner, J. H., Herdegen, V., Repke, J.-U., & Spitzer, K. (2013). The impact of CO₂ on the electrical properties of water bearing porous media-laboratory experiments with respect to carbon capture and storage. *Geophysical Prospecting*, 61, 446–460.
- Börner, J. H., Herdegen, V., Repke, J.-U., & Spitzer, K. (2015). The electrical conductivity of CO₂-bearing pore waters at elevated pressure and temperature: A laboratory study and its implications in CO₂ storage monitoring and leakage detection. *Geophysical Journal International*, 203, 1072–1084.
- Börner, J. H., Herdegen, V., Repke, J.-U., & Spitzer, K. (2017). Spectral induced polarization of the three-phase system CO₂–brine–sand under reservoir conditions. *Geophysical Journal International*, 208(1), 289–305.
- Breede, K., Kemna, A., Esser, O., Zimmermann, E., Vereecken, H., & Huisman, J. A. (2012). Spectral induced polarization measurements on variably saturated sand-clay mixtures. *Near Surface Geophysics*, 10, 479–489.
- Cole, K. S., & Cole, R. H. (1941). Dispersion and absorption in dielectrics I. Alternating current characteristics. *The Journal of Chemical Physics*, 9, 341–351.
- Duba, A., Huengest, E., Nover, G., Will, G., & Jödicke, H. (1988). Impedance of black shale from Münsterland 1 borehole: An anomalously good conductor? *Geophysical Journal International*, 94(3), 413–419.
- Esposito, R., Troiano, A., Di Giuseppe, M. G., Patella, D., & Castelo Branco, R. (2017). The magnetotelluric response over a 3D polarizable structure. *Journal of Geophysics and Engineering*, 14(3), 698.
- Girault, F., Bollinger, L., Bhattarai, M., Koirala, B., France-Lanord, C., Rajaure, S., et al. (2014). Large-scale organization of carbon dioxide discharge in the Nepal Himalayas. *Geophysical Research Letters*, 41, 6358–6366. <https://doi.org/10.1002/2014GL060873>
- Girault, F., Perrier, F., Gajurel, A. P., Bhattarai, M., Koirala, B. P., Bollinger, L., et al. (2012). Effective radium concentration across the Main Central Thrust in the Nepal Himalayas. *Geochimica et Cosmochimica Acta*, 98, 203–227.
- Groppo, C., Rolfo, F., Castelli, D., & Connolly, J. A. D. (2013). Metamorphic CO₂ production from calc-silicate rocks via garnet-forming reactions in the CFAS-H₂O-CO₂ system. *Contributions to Mineralogy and Petrology*, 166, 1655–1675.
- Israil, M., Tyagi, D., Gupta, P., & Niwas, S. (2008). Magnetotelluric investigations for imaging electrical structure of Garhwal Himalayan corridor, Uttarakhand, India. *Journal of Earth System Science*, 117(3), 189–200.
- Jödicke, H. (1992). Water and graphite in the Earth's crust—An approach to interpretation of conductivity models. *Surveys in Geophysics*, 13(4), 381–407.
- Jödicke, H., Kruhl, J. H., Ballhaus, C., Giese, P., & Untiedt, J. (2004). Syngenetic, thin graphite-rich horizons in lower crustal rocks from the Serre San Bruno, Calabria (Italy), and implications for the nature of high-conducting deep crustal layers. *Physics of the Earth and Planetary Interiors*, 141(1), 37–58.
- Kohn, M. J., Paul, S. K., & Corrie, S. L. (2010). The lower Lesser Himalayan sequence: A Paleoproterozoic arc on the northern margin of the Indian plate. *Geological Society of America Bulletin*, 122(3–4), 323–335.
- Lemonnier, C., Marquis, G., Perrier, F., Avouac, J.-P., Chitrakar, G., Kafle, B., et al. (1999). Electrical structure of the Himalaya of central Nepal: high conductivity around mid-crustal ramp along the MHT. *Geophysical Research Letters*, 26(21), 3261–3264.
- Manca, G., & Viezzoli, A. (2018). A thorough synthetic study on IP effects in AEM data from different systems, ASEG Extended Abstracts, 7.
- Marchant, D., Kang, S., McMillian, M., & Haber, E. (2018). Modelling IP effects in airborne time domain electromagnetics, ASEG Extended Abstracts, 6.
- Olhoeft, G. R. (1979). Electrical properties, initial report of the petrophysics laboratory. Circular 789, U.S. Geological Survey.
- Pavan Kumar, G., Manglik, A., & Thiagarajan, S. (2014). Crustal geoelectric structure of the Sikkim Himalaya and adjoining Gangetic foreland basin. *Tectonophysics*, 637, 238–250.
- Pelton, W., Ward, S., Hallof, P., Sill, W., & Nelson, P. (1978). Mineral discrimination and removal of inductive coupling with multifrequency IP. *Geophysics*, 43(3), 588–609.
- Rawat, G., Arora, B. R., & Gupta, P. K. (2014). Electrical resistivity cross-section across the Garhwal Himalaya: Proxy to fluid-seismicity linkage. *Tectonophysics*, 637, 68–79.
- Revil, A., Florsch, N., & Mao, D. (2015). Induced polarization response of porous media with metallic particles—Part 1: A theory for disseminated semiconductors. *Geophysics*, 80(5), D525–D538.

- Revil, A., & Skold, M. (2011). Salinity dependence of spectral induced polarization in sands and sandstones. *Geophysical Journal International*, *187*, 813–824.
- Sailhac, P., Larnier, H., Bano, M., Adhikari, L. B., Bollinger, L., Perrier, F., et al. (2016). Magnetotelluric survey in the quest for crustal conductivities in Nepal after the Mw 7.9 Gorkha earthquake of April 25, 2015. Abstract GP34A-03 Presented at the 2016 AGU Fall Meeting, San Francisco, CA.
- Sapkota, S. N., Bollinger, L., Klinger, Y., Tapponnier, P., Gaudemer, Y., & Tiwari, D. (2013). Primary surface ruptures of the great Himalayan earthquakes in 1934 and 1255. *Nature Geoscience*, *6*(1), 71–76.
- Schön, J. (2015). *Physical properties of rocks—Fundamentals and principles of petrophysics, handbook of geophysical exploration* (Vol. 65). Amsterdam: Elsevier.
- Skold, M., Revil, A., & Vaudelet, P. (2011). The pH dependence of spectral induced polarization of silica sands: Experiment and modeling. *Geophysical Research Letters*, *38*, L12304. <https://doi.org/10.1029/2011GL047748>
- Stoyer, C. H. (1976). Consequences of induced polarization in magneto-telluric interpretation. *Pure and Applied Geophysics*, *114*(3), 435–449.
- Unsworth, M. (2010). Magnetotelluric studies of active continent–continent collisions. *Surveys in Geophysics*, *31*(2), 137–161.
- Unsworth, M. J., Jones, A. G., Wei, W., Marquis, G., Gokarn, S. G., Spratt, J. E., & INDEPTH-MT team (2005). Crustal rheology of the Himalaya and Southern Tibet inferred from magnetotelluric data. *Nature*, *438*, 78.
- Upreti, B. N. (1999). An overview of the stratigraphy and tectonics of the Nepal Himalaya. *Journal of Asian Earth Sciences*, *17*(5), 577–606.
- Vinegar, H. J., & Waxman, M. H. (1984). Induced polarization of shaly sands. *Geophysics*, *49*(8), 1267–1287.
- Warburg, E. G. (1899). *Annalen der Physik und Chemie. Neue Folge 67 (Annalen der Physik. Band 303), chap. Ueber das Verhalten sogenannter unpolarisierbarer Elektroden gegen Wechselstrom* (pp. 493–499). Leipzig: Verlag von Johann Ambrosius Barth.
- Waxman, M. H., & Smits, L. J. M. (1968). Electrical conductivities in oil-bearing shaly sands. *Society of Petroleum Engineers Journal*, *8*, 107–122.
- Weller, A., & Slater, L. (2012). Salinity dependence of complex conductivity of unconsolidated and consolidated materials: Comparisons with electrical double layer models. *Geophysics*, *77*(5), D185–D198.